Climatic Regimes of Tropical Convection and Rainfall

BIN WANG

Department of Meteorology, School of Ocean and Earth Science and Technology, University of Hawaii, Honolulu, Hawaii

(Manuscript received 3 July 1992, in final form 10 May 1993)

ABSTRACT

Annual distribution and phase propagation of tropical convection are delineated using harmonic and amplitude-phase characteristics analysis of climatological pentad mean outgoing longwave radiation and monthly frequencies of highly reflective cloud.

An annual eastward propagation of peak rainy season along the equator from the central Indian Ocean (60°E) to Arafura Sea (130°E) is revealed. This indicates a transition from the withdrawal of the Indian summer monsoon to the onset of the Australian summer monsoon. Significant bimodal variations are found around major summer monsoon regions. These variations originate from the interference of two adjacent regimes.

The convergence zones over the eastern North Pacific, the South Pacific, and the southwest Indian Ocean are identified as a marine monsoon regime that is characterized by a unimodal variation with a concentrated summer rainfall associated with the development of surface westerlies equatorward of a monsoon trough. Conversely, the central North Pacific and North Atlantic convergence zones between persistent northeast and southeast trades are classified as trade-wind convergence zones, which differ from the marine monsoon regime by their persistent rainy season and characteristic bimodal variation with peak rainy seasons occurring in late spring and fall.

The roles of the annual march of sea surface temperature in the phase propagation and formation of various climatic regimes of tropical convection are also discussed.

1. Introduction

The latent heat released in convective clouds drives the tropical atmosphere and influences global atmospheric circulation. Unfortunately, tropical convection and accompanying diabatic heating have not been modeled with an acceptable fidelity by atmospheric general circulation models (GCMs) and climate models. There is a keen need to understand the variations of tropical convection on various time scales.

Although general characteristics of the *annual variation* of precipitation for global continents and islands have been well documented (e.g., Kendrew 1961; Hsu and Wallace 1976), little is known about the temporal and spatial fluctuations of precipitation over tropical oceans. Prior to the 1980s, major efforts had been made to study the annual cycle of precipitation over tropical oceans by use of rainfall measurements over islands (Tucker 1961; Taylor 1973) and ocean weather stations (Reed and Elliott 1973) as well as ship reports (Dorman and Bourke 1979, 1981). These analyses provided valuable preliminary information, but in view of the inhomogeneous and insufficient spatial and temporal coverage of the data, climatological behavior of rainfall must be ascertained using a more complete dataset.

In this connection, indirect estimates of rainfall, based on observations of clouds in visible and thermal infrared imagery, have been used extensively. A thorough review of this subject can be found in Arkin and Ardanuy (1989). In the last decade, outgoing longwave radiation (OLR) data have been widely used in deducing annual cycles of convection and rainfall in the tropical Pacific and Indian oceans (Horel 1982; Meehl 1987; Murakami and Wang 1993), tropical America (Horel et al. 1989), and the global tropics (Heddinghaus and Krueger 1981; Wolter and Hastenrath 1989; Mitchell and Wallace 1992).

Most climate studies of tropical convection have been focused on specific or regional features. Details of phase propagation and seasonal distribution of the field over vast ocean areas have not been systematically explored. Consequently, climatic regimes of tropical convection have not been objectively and precisely delineated. The present study is aimed at analyzing and interpreting large-scale characteristics of the annual variation of tropical convection. Section 2 describes the data used for inferring convection and analysis procedures. Sections 3 and 4 investigate, respectively, the annual propagation of the peak and the onset phases of rainy (or wet) seasons and the seasonal distribution over the global tropics. A classification of the annual cycle of tropical convection is attempted in section 5.

Corresponding author address: Dr. Bin Wang, Department of Meteorology, School of Ocean and Earth Sciences and Technology, University of Hawaii at Manoa, 2525 Correa Road, Honolulu, HI 96822.

The influences of sea surface temperature (SST) on the annual cycle of tropical convection and the limitations of the present analysis are discussed in the last section.

2. Data and methodology

a. Datasets

The principal datasets used to infer tropical convection and rainfall are climatological pentad mean OLR and monthly frequency of highly reflective clouds (HRC) (number of days with HRC per month). The pentad mean OLR data were obtained from the Climate Analysis Center/NMC (National Meteorological Center). The data are on a 2.5 × 2.5° grid and cover the period from June 1974 to December 1989 with a gap from March to December 1978. The original production and organization of the data, for example, the treatment of the inhomogeneities arising from the differences in satellites and equatorial crossing times, were documented by Gruber and Krueger (1984). The HRC data were created by Garcia (1985) by subjectively analyzing daily visible and infrared polar-orbiting satellite mosaics to identify deep, organized convective systems (cloud clusters), which are responsible for most tropical rainfall (Kilonsky and Ramage 1976). The HRC data have a resolution of 1° × 1° grid and cover the period from January 1971 to July 1987 for the global tropics between 25°N and 25°S. For the purpose of describing large-scale features, climatological pentad mean OLR were calculated for a coarser resolution of 5° × 5°.

Both OLR and HRC data were derived from the same satellites and have homogeneous spatial sampling, relatively high temporal and spatial resolution, and a full coverage for the tropics. As indices for convection and rainfall, however, both data must be used with caution. The OLR data are subject to contaminations from cirrus clouds (Morrissey 1986; Yoo and Carton 1988) and from surface temperature and atmospheric moisture content. The latter are severe in cloud-free regions and over mountains. The HRC data were designed to exclude the aforementioned contaminations but the analyses contain subjective biases. The HRC data are also affected by mean diurnal cycles of convection over different regions of the tropics and tend to underestimate HRC frequency over land (Garcia 1985). In view of the above, the present analyses, when possible and adequate, have been carried out in parallel using both datasets. Conclusions were drawn through careful comparison of the results derived from each dataset.

Except for arid regions and the northeast Pacific, monthly HRC and OLR are well correlated on monthly time scales. The linear correlation coefficients range from −0.65 to −0.85. Sample size is 150 at each 2° × 2° square. The statistical relationship between monthly mean OLR and rainfall was studied by Morrissey (1986), Motell and Weare (1987), Yoo and Carton (1988), and others. The relationship between HRC and rainfall was examined by Kilonsky and Ramage (1976). A summary of these statistical relationships among OLR, HRC, and rainfall suggests that a monthly mean OLR of 240 W m^{-2} corresponds roughly to a HRC frequency of 3 days $month^{-1}$ and a rainfall amount of 210 mm $month^{-1}$. Anomalous monthly mean OLR of 15 W m^{-2} corresponds approximately to an HRC anomaly of 1 day $month^{-1}$ and a rainfall anomaly of 80 mm $month^{-1}$.

b. Harmonic and phase-amplitude characteristics analysis

In order to objectively depict annual distribution and to determine the boundaries of various climatic regimes, a popular approach adopted in the literature is harmonic analysis (e.g., Horn and Bryson 1960; Hastenrath 1968; Hsu and Wallace 1976). This method provides a convenient vector form for displaying annual and semiannual Fourier harmonics. Problems arise from separation of harmonics. Significant amplitude of the semiannual Fourier harmonic can be a result of asymmetry of the annual cycle. For instance, a short and intensive summer rainy season versus a long and "flat" dry season yields a semiannual Fourier harmonic with considerable amplitude, although there is no *apparent* semiannual variation.

Besides harmonic analysis, the present study also analyzes phase–amplitude characteristics of the annual cycle without a harmonic decomposition, following Mokhov (1985). To eliminate short-period (less than a season) fluctuations, a smoothed annual cycle is reconstructed by taking the sum of the annual mean and the first (annual) and second (semiannual) harmonics of climatological pentad mean series. The smoothed annual cycle is either unimodal (single maximum and minimum) or bimodal (double maxima and minima). Figure 1 presents an example of a bimodal annual cycle. The annual range and apparent semiannual range are defined, respectively, by the difference between the primary maximum and minimum and that between the secondary maximum and minimum. The ratio of the

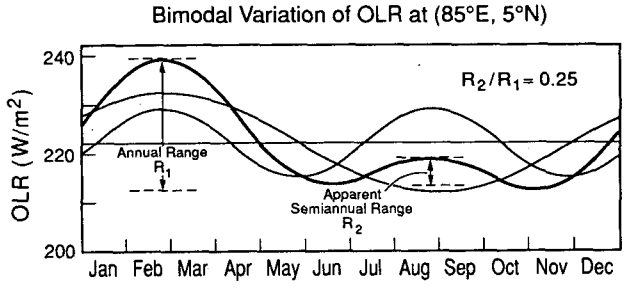

FIG. 1. Bimodal annual cycle of pentad mean OLR (thick solid) and the corresponding components of the annual mean, annual, and semiannual harmonics at (5°N, 85°E), south of Sri Lanka.

semiannual to annual range provides an objective index for measuring the degree of unimodal or bimodal behavior. The minimum ratio is zero, which means a unimodal variation. The maximum ratio is unity, which implies a "perfect" bimodal variation, that is, the two maxima (or minima) are equal.

Because the analysis is based on the smoothed annual cycle, its representativeness should be inspected. The fractional variance carried by each Fourier harmonic is

$$V_i = C_i^2/(2V_t), \quad i = 1, 2,$$

where C_i is the amplitude of the ith harmonic and V_t the total variance of the annual cycle. The quantity, $V_1 + V_2$, represents the fractional variance carried by the smoothed annual cycle. Figure 2a displays spatial variabilities of the fractional variance of smoothed OLR annual cycle. In general, the fractional variance is highly correlated with its annual range (Fig. 2b). In most regions where annual range is less than 15 W m^{-2}, more than one-half of the annual variance is carried by short-period fluctuations, whereas in the regions where annual range exceeds 30 W m^{-2}, the annual variations are dominated by the annual and semiannual harmonics. Figure 2 indicates that in most regions of the tropics the smoothed annual cycle accounts for more than 60% of the total variance of the climatological pentad mean series.

3. Annual phase propagation

a. Propagation of the peak wet season

Figure 3 presents an overview of the timing of local annual minimum OLR at different geographic locations, which portrays the phase propagation of the local peak wet season. The regions in which peak wet seasons occur nearly concurrently may be considered as belonging to the same regime. These regions include 1) South Asia and northwest tropical Pacific (July–August); 2) central North Africa (August); 3) eastern North Pacific and Central America (July); 4) northern Australia–southwest tropical Pacific (January–February); 5) southern Africa and southwest Indian Ocean (January–February); 6) central South America (January–February); 7) equatorial eastern Pacific (March); 8) equatorial Atlantic (March); 9) subtropical North Atlantic (October–November); and 10) subtropical central North Pacific (October). Regions 1–6 all display a peak rainy season in summer that is indicative of a summer monsoon climate. Regions 7 and 8 exhibit a distinctive equatorial regime, having a single well-defined wet season in boreal spring. In contrast, the peak wet seasons in region 9 and 10 occur in northern fall.

Phase discontinuity between the uniform-phase regions provides natural boundaries for different regimes. There exist, however, transitional regions in which phase changes more gradually from one uniform-phase

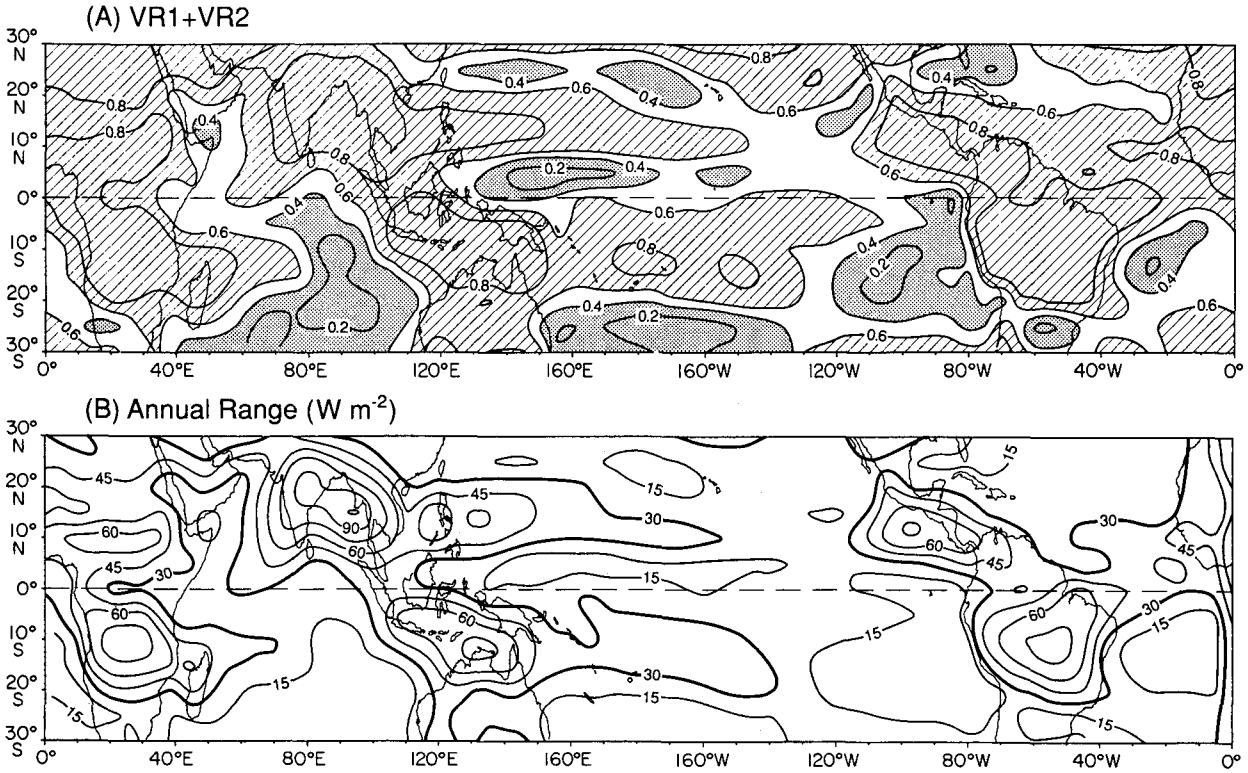

FIG. 2. Contour plot of (a) the sum of the fractional variance of the annual ($VR1$) and semiannual ($VR2$) harmonics, and (b) the annual range of the reconstructed annual cycle of pentad mean OLR.

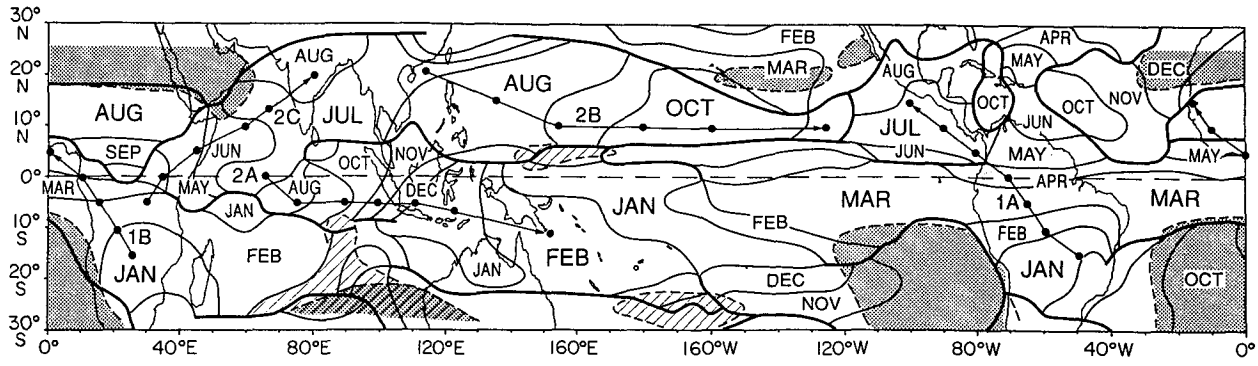

FIG. 3. Phase diagram for the annual minimum pentad mean OLR. The thick solid lines denote discontinuous isochrones, across which the phase differs by at least 12 pentads (2 months). Routes 1A, 1B, 2A, 2B, and 2C indicate phase propagations. Extremely dry regions with the maximum monthly HRC frequency less than 0.5 day month^{-1} and regions with the fractional variance of the reconstructed annual cycle less than 0.2 are marked out by the meshed and hatched areas, respectively.

region to another. These gradual phase transitions depict several major phase propagation routes (Fig. 3).

Over both the American and African sectors the peak wet season occurs progressively later northwestward from southern subtropics in January to northern subtropics in August (route 1A and 1B, Fig. 3). Although equatorial South America and Africa have double peak rainy seasons, the April peak is generally stronger than the October one.

A noticeable slow eastward phase propagation is observed from the equatorial central Indian Ocean (60°E) to the Arafura Sea (130°E) from August to January (route 2A, Fig. 3). This is confirmed by the annual variation of monthly HRC frequency along the latitude band between the equator and 5°S (figure not shown). Murakami et al. (1992) pointed out that during northern summer the grand Hadley circulation along 90°E consists of two cells: a major Northern Hemisphere cell and a minor Southern Hemisphere cell. The northern cell is mainly driven by land–ocean thermal contrast with a strong updraft in the Indian monsoon trough around 20°N and a weak downdraft around 5°N. The southern cell is partially supported by the large SST gradients between 20°S and 10°S with an ascending branch around 5°S and a descending branch between 20° and 30°S. In September, the updraft of the northern cell in the Indian monsoon region suddenly weakens. Concurrently, convection increases rapidly and forms a new convective maximum just south of the equator in the updraft of the southern cell. From October to January of the next year this convection maximum moves eastward from 95°E to 120°E in harmony with the development of the Indonesian and Australian monsoon. The eastward phase propagation of the peak wet season from August to January as seen in Fig. 3 reflects the transition from the northern summer monsoon to the southern summer monsoon in South Asia–Australia. Using OLR averaged between 30°N and 30°S, Meehl (1987) showed an annual eastward propagation from India to the eastern Pacific. That eastward propagation averaged for the broad latitude band was dominated by monsoonal rainfall in India, northern Australia, and western Pacific. The eastward propagation of the peak rainy season described here is a near-equatorial phenomenon.

A significant eastward propagation also occurs from the Philippines to north of the central Pacific intertropical convergence zone (ITCZ). The peak wet season occurs in late July at northern Philippines, in August over the Philippine Sea, in September around 10°N, 160°E, and in October over the central Pacific ITCZ (10°N, 160°W) (route 2B, Fig. 3). This route is in consonance with the withdrawal of the western Pacific monsoon trough and the enhanced tropical cyclone activity near the date line during northern fall.

A northeastward propagation is evident from equatorial Africa, via Somalia and the Arabian Sea, to the Indian subcontinent, providing a linkage between African equatorial convection and Indian monsoon rains (route 2C, Fig. 3). Although there is no continuous movement of a convective maximum along this route due to the subsidence over the cold water off Somalia, the progressive phase lag in the peak wet season from equatorial Africa to India is robust. This phase propagation is consistent with the northeastward migration of convection in eastern Africa from April to May and with the subsequent convective development southwest of India around the Laccadive islands (10°N, 70°E) in June. The latter is often accompanied by the development of the onset vortex of the Indian summer monsoon.

b. Annual march of the rainy season

The period in which the smoothed pentad mean OLR is lower than or equal to 230 W m^{-2} is defined as the rainy season. The first and last pentad of the rainy season is, respectively, referred to as the time of onset and withdrawal of rainy season. Such a definition

is in reasonable agreement with those determined using land-based rainfall data in the Asian monsoon region (Ramage 1971) or using OLR data in tropical America (Horel et al. 1989).

Over Africa, the local rainy season starts progressively later poleward from the equatorial permanent convection region (Fig. 4a). In addition, there are components directed southeastward to Madagascar and northwestward to off the coast of Guinea. Over the American sector the onset phase propagates primarily southeastward in the Southern Hemisphere and northwestward in the Northern Hemisphere.

In the South Asia–Australia sector, however, both northwest and northeast propagation occur in the Northern Hemisphere and zonal propagation is more prominent in the Southern Hemisphere. Over South Asia, the rainy season begins at the northern tip of Sumatra in early April and progressively later northwestward to northwest India in early July. This phase propagation reflects the annual march of a massive convection area during the same period. Inspection of the HRC atlas of Garcia (1985) reveals that from April to May an HRC maximum in the equatorial eastern Indian Ocean (2°N, 95°E) shifts to northern Sumatra and the southern Andaman Sea (10°N, 95°E). Thereafter the HRC maximum moves steadily northward along the west coast of Burma until August when it reaches its northernmost position in the head of the Bay of Bengal (90°E, 18°N). Over the South China Sea and Philippine Sea, on the other hand, the onset of rainy season starts at northern Borneo in May and progressively later northeastward to the eastern Philippine Sea in August, corresponding to the seasonal migration of the monsoon trough as seen from the atlas of Sadler et al. (1987). In the Southern Hemisphere, the onset phase of the rainy season propagates eastward from the equatorial eastern Indian Ocean (in September) to the Arafura Sea (in December), similar to the propagation of the peak rainy season (Fig. 3). In the southwest Pacific, the onset phase propagation follows the seasonal extension of South Pacific convergence zone (SPCZ) from (10°S, 160°E) to (15°S, 160°W).

The withdrawal phase is nearly a function of latitude except near the equator (Fig. 4b).

4. Unimodal and bimodal variation

Two indices are used to qualitatively delineate unimodal/bimodal variation of OLR. The first is the ratio of semiannual to annual range, R_2/R_1, which is contoured in Fig. 5a. The other is the difference in fractional variances between the annual and semiannual

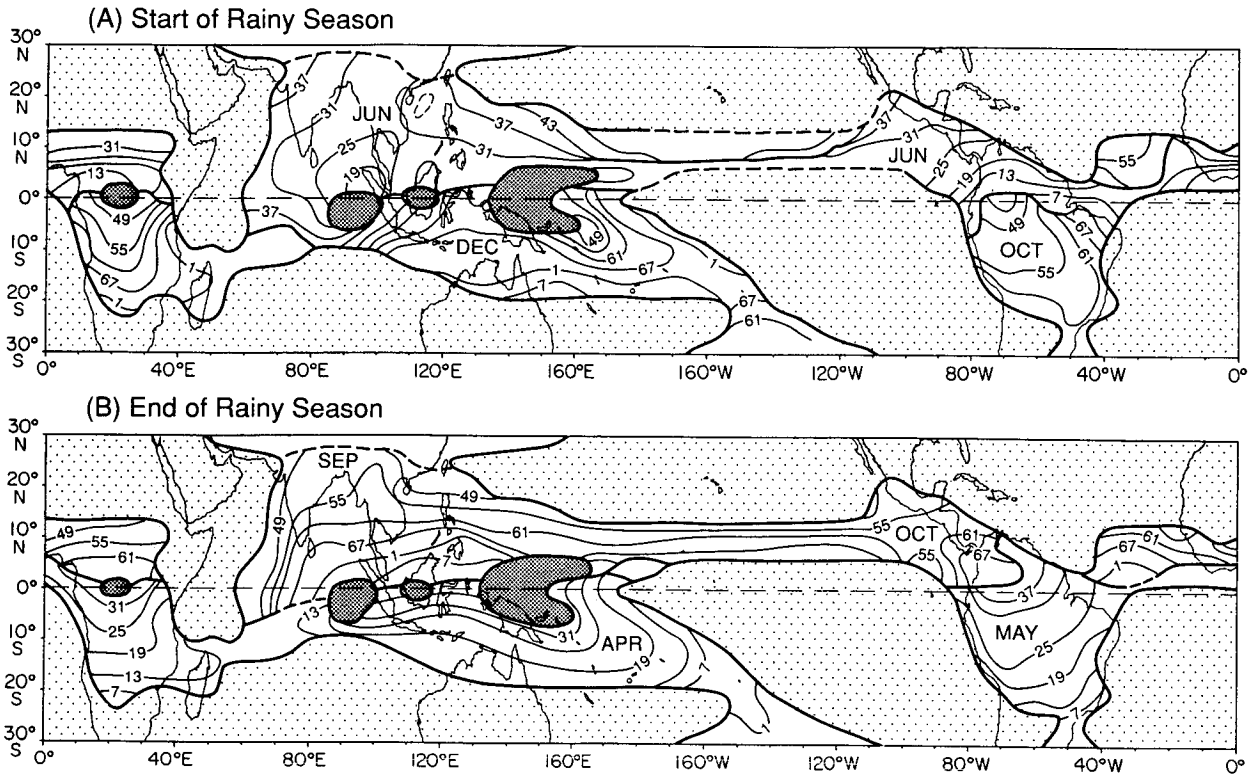

FIG. 4. Phase diagram for (a) the onset and (b) withdrawal of the local rainy season computed using reconstructed OLR annual cycles. Thin solid contours are isochrones with labels indicating the number of the pentad associated with the beginning and end of rainy season. Light meshed shading areas are dry areas where climatological pentad mean OLR is higher than 230 W m^{-2} all year round. Dark meshed shading areas represent regions with a year-round pentad mean OLR lower than 230 W m^{-2}.

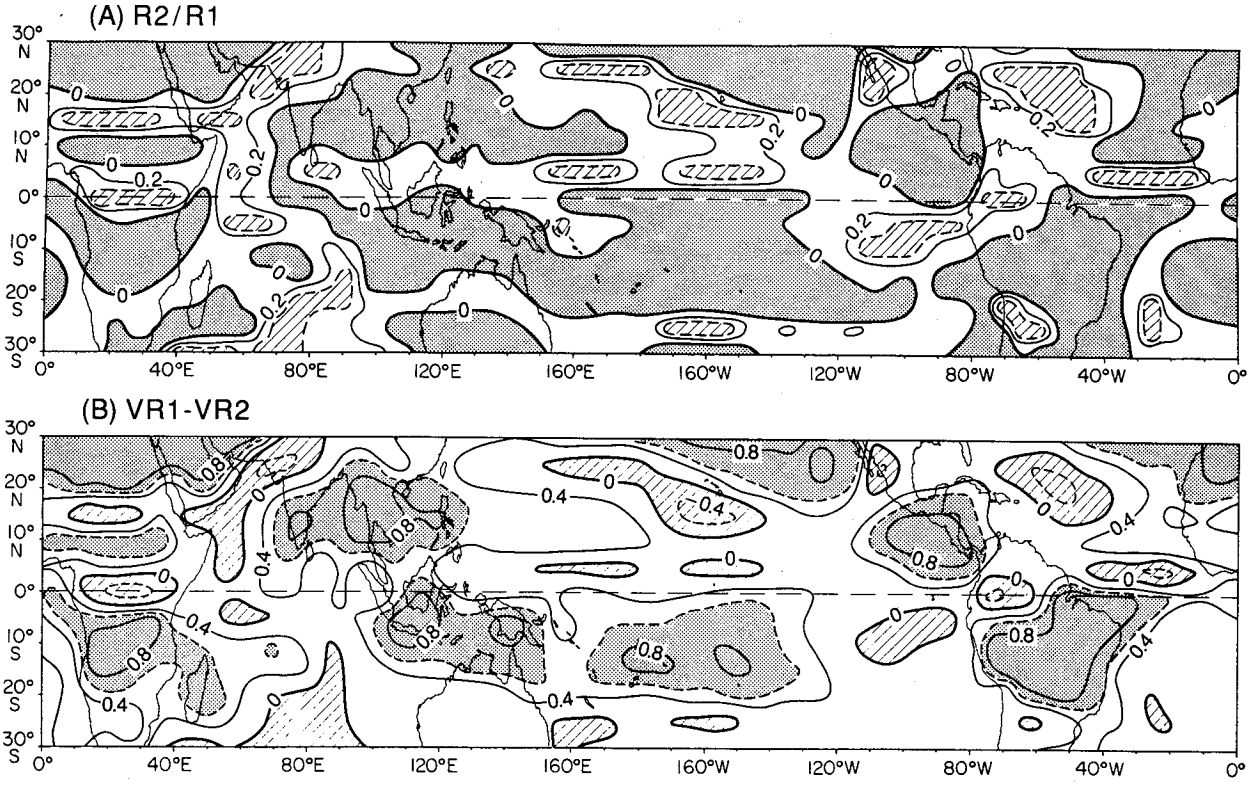

FIG. 5. Contour plot of (a) the ratio of semiannual to annual arrange, $R2/R1$, and (b) the fractional variance difference between the annual ($VR1$) and semiannual ($VR2$) harmonics, $VR1-VR2$. In (a) the regions with unimodal ($R2/R1 = 0$) and significant bimodal ($R2/R1 \geq 0.2$) variations are marked by meshed and hatched area, respectively.

harmonics, $V_1 - V_2$, shown in Fig. 5b. The second index is conventionally used in harmonic analysis (e.g., Scott and Shulman 1979). Qualitative agreement between Figs. 5a and 5b is obvious. Negative values of $V_1 - V_2$ generally correspond well to an R_2/R_1 exceeding 0.2, suggesting that a negative $V_1 - V_2$ in harmonic analysis implies a significant apparent bimodal variation. Some bimodal variations (the one shown in Fig. 1 for example), however, are well depicted by R_2/R_1 (0.25 for the case in Fig. 1) but not by the harmonic index (about 0.4 in Fig. 1).

Comparison of the phase diagram for peak wet season (Fig. 3) and the diagram for the ratio of semiannual to annual range (Fig. 5a) reveals that the regions of uniform phase correspond very well to the regions of unimodal variation, whereas the discontinuity in the phase diagram often occurs in the regions of bimodal variation. The latter tend to surround principal summer monsoon regions, especially in the Northern Hemisphere (Fig. 5).

In equatorial Africa and South America, bimodal variations in OLR occur in a narrow latitudinal belt that separates Northern and Southern Hemisphere summer monsoon regions. This agrees with Kendrew's (1961) equatorial regime of precipitation. Between South Asian and Australian summer monsoons there also exists a narrow zone with weak bimodal variation along 5°N from south of Sri Lanka to northern Borneo (70°E–120°E) (Fig. 5a). Minimum OLR occurs in May and October–November, respectively (Fig. 1). The May rainy season is associated with the onset of the summer (southwest) monsoon whereas the November rainy season results from the equatorward intrusion of the winter (northeast) monsoon.

Bimodal variations are also found in the mean positions of the North Pacific and North Atlantic ITCZs. Examples are shown in Fig. 6a. The double OLR minima occurring in May and November are apparently associated with the annual march of the ITCZs.

Other regions of significant bimodal variation are located in the subtropics. Comparison of Fig. 5 with Fig. 3 indicates that these regions coincide well with the regions of phase discontinuity, suggesting that the bimodal variations are caused by interference from two adjacent regimes. Significant bimodal variations occurring in the northern subtropics (10°–25°N) between summer monsoon and arid subtropical regions are good examples. Annual cycles of OLR in these regions are shown in Fig. 6b. In the northern Arabian Sea (20°N, 65°E) and south of Baja California (20°N, 110°W), the alternate influences of summer monsoon (the Indian monsoon and eastern North Pacific mon-

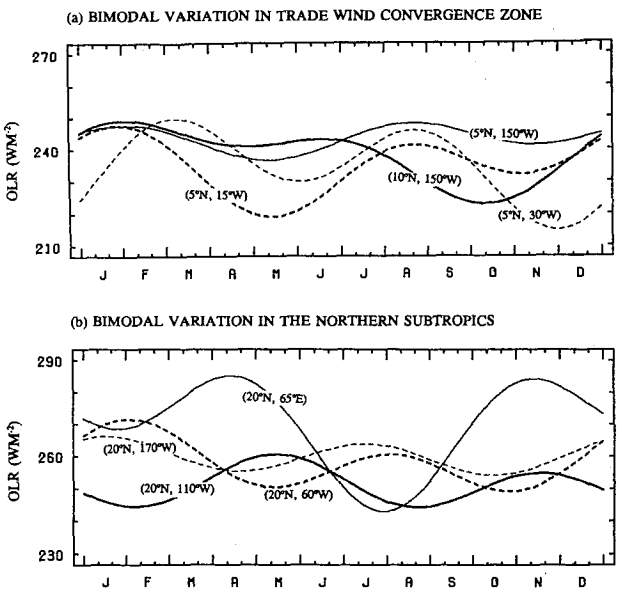

FIG. 6. Reconstructed annual cycles of pentad mean OLR depicting bimodal variations in (a) trade-wind convergence zones, and (b) Northern Hemisphere subtropics.

soon) and midlatitude winter conditions [Mediterranean regime as termed by Kendrew (1961)] are responsible for the peak rainy seasons in July and January, respectively. In the subtropical mid-North Pacific (20°N, 170°W) and mid-North Atlantic (20°N, 60°W) trade winds prevail year round and the climate is relatively dry. The double wet seasons occurring in late spring and late fall are features for intriguing speculation. At the mid-North Pacific, the minimum OLR in October occurs when the ITCZ is in its northernmost position and the local SST reaches its annual maximum. The secondary minimum OLR in April may be related to the seasonal change of the upper-tropospheric subtropical jet. Sadler (1975) noticed that the April peak in rainfall near the Hawaiian Islands is associated with a major change in the upper-tropospheric flow: the maximum speed axis in the westerlies moves southward through the islands from March to April and speeds at the axis are greatest in April. East of Puerto Rico (20°N, 60°W) October–November minimum OLR is usually attributed to the occurrence of tropical cyclones. The May wet season was speculated to be a result of the southward migration of the maximum axis of a upper-level westerly jet into the Caribbean in May (Sadler 1975).

5. Climatic regimes

It is, in general, more meaningful to categorize climatic regimes of tropical convection based on the synthesis of essential characteristics of the annual cycles of OLR or HRC, which include 1) seasonal distribution, 2) the peak phase and duration of the rainy (or wet) season, and 3) the extreme and the range of the annual cycle. Based on these characteristics, four climatic regimes for tropical convection can be identified. Their geographic distribution is shown in Fig. 7 and their principal indices are given in Table 1.

a. Arid and semiarid regimes

The dry (arid and semiarid) regimes have no rainy season and are defined by an annual maximum HRC frequency less than or equal to three days month^{-1} (or equivalently, an annual minimum pentad mean OLR higher than 230 W m^{-2}). The area where the maximum HRC frequency is less than 0.5 day month^{-1} indicates an extremely dry climate that is referred to as the arid regime, distinguished from other dry regions (semiarid regime). Most (not all) semiarid areas exhibit bimodal variation (Fig. 5).

b. Equatorial permanent and semipermanent convective regimes

Wet (permanent and semipermanent convection) regimes have no significant dry season. Regions with

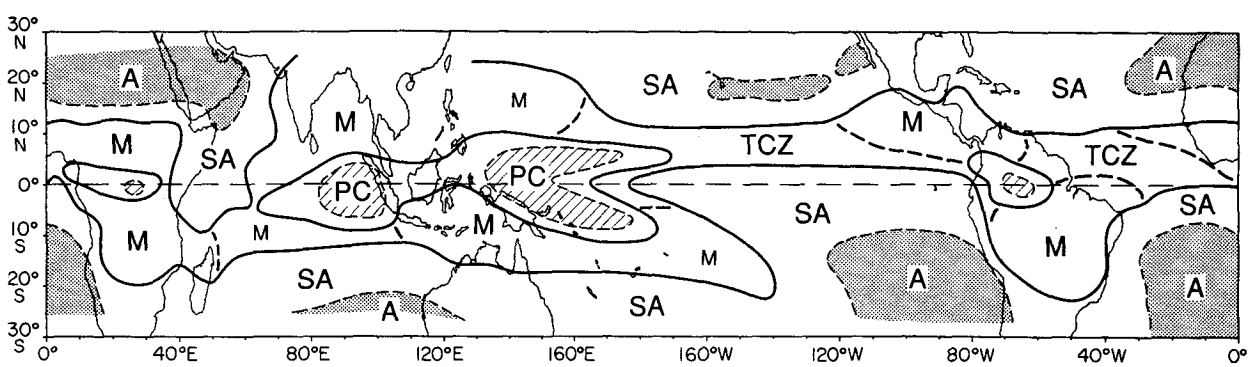

FIG. 7. Climatic regime diagram for tropical convection/rainfall. Letters A, SA, PC, M, and TCZ represent, respectively, arid, semiarid, permanent convective, summer monsoon, and trade-wind convergence zone. The hatched (meshed) shading denotes permanent convective (arid) regions.

TABLE 1.

Convection regimes	Dry		Monsoon		Trade-wind convergence zone	Wet	
	Arid	Semiarid	Strong	Moderate		Semipermanent	Permanent
Maximum HRC freq.	<0.5	0.5–3	>5	3–5	>4	>5	>5
Minimum HRC freq.	<1		<2		<2	2–3	>3
Annual range of HRC freq. (day mo^{-1})	<0.5	<3	>5	3–5	3–5	<5	
Seasonal distribution	Unimodal	mixed	Unimodal		Bimodal	Bimodal	
Duration of rainy season (mos)	0		3–6		>7	>8	12
Peak rainy season	Summer				Fall or spring	Equinoctial seasons	
Circulation system	Trade winds	Trade winds	Monsoon troughs	SPCZ/ SWICZ	TWCZ	Equatorial troughs	

persistent rainfall throughout the year belong to a permanent convective regime that can be defined by an annual minimum HRC frequency greater than three days month^{-1} (or an annual maximum pentad mean OLR below 230 W m^{-2}). The surroundings of the permanent convection areas have an annual minimum HRC frequency higher than two days month^{-1} (or annual maximum pentad mean OLR lower than 240 W m^{-2}) and may be signified as semipermanent convection regions, in which the rainy season is normally longer than ten months. For both wet regimes bimodal variation is often observed and the seasonal fluctuation of convection is moderate: the annual range of HRC frequency is less than 3 days month^{-1}.

c. *Summer monsoon regime*

The summer monsoon regime is characterized by 1) a unimodal seasonal distribution, 2) an intense rainy season (the maximum HRC frequency is greater than 5 days month^{-1} or the minimum pentad mean OLR is lower than 220 W m^{-2}) occurring in summer, and 3) a large annual amplitude. The annual range of HRC (pentad mean OLR) generally exceeds 5 days month^{-1} (45 W m^{-2}). Major monsoon regions are located at both sides of the equatorial wet regimes (Fig. 7). Monsoon troughs and monsoon depressions or tropical storms are major rain-producing weather systems in all major monsoon regions.

The southeast SPCZ and southwest Indian Ocean convergence zone (SWICZ) display many features in common with the major monsoon regions. All three characteristics of monsoonal rainfall are met except a weaker intensity of rainy season (maximum HRC frequency is three to five days month^{-1}) and a slightly smaller annual range. It is, therefore, reasonable to classify these two oceanic convergence zones as marine monsoon regions.

d. *The regime of trade-wind convergence zone (TWCZ)*

This regime includes the central North Pacific and North Atlantic ITCZ. The annual range of pentad mean OLR is 20–40 W m^{-2} and that of HRC frequency is 3–4 days month^{-1}. These values are greater than those for both dry and wet regions but smaller than those for major monsoon regions. The annual cycle of OLR is bimodal with peak rainy seasons occurring in May and October/November, respectively (Fig. 6a). The rainy season is less intense compared to major summer monsoons with a maximum HRC frequency below or around 5 days month^{-1}. The rainy season duration, however, is substantially longer than that of the monsoon regime.

The TWCZ also differs from oceanic monsoon regions in surface wind fields. In all four oceanic monsoon regions (the western North Pacific, the eastern North Pacific, the southeast part of the SPCZ, and the SWICZ), the summer monsoon rains are produced within monsoon troughs. The surface winds located on the equatorward side of a monsoon trough reverse their directions between summer and winter. The maximum convergence and convection are associated with the eastward and/or poleward wind component (summer monsoon flow) on the equatorward side of the monsoon troughs. It follows that the convection has a unimodal annual variation with the rainy season in phase with summer monsoon westerlies. Conversely, the TWCZ is a narrow confluent zone of dry northeast and southeast trades of respective hemispheres. The winds on both side of the TWCZ are easterlies all year round. The maximum convection occurs where the northeast and southeast trades converge.

To further illustrate the difference between the marine monsoon and TWCZ, month-to-month variations of surface winds along 7°N and HRC frequency averaged between 7°N and 9°N across the Pacific Ocean are shown in Fig. 8. Notice that the ITCZ east of 125°W differs from that west of 125°W. Summer monsoons (southwesterlies) are observed in the eastern North Pacific (120°W–90°W) as well as in the western North Pacific (125°E–155°E) where heavy rainfall is concentrated in summer (June to August) with maximum monthly HRC higher than 6 days per month. In the central North Pacific between 160°E and 130°W, on

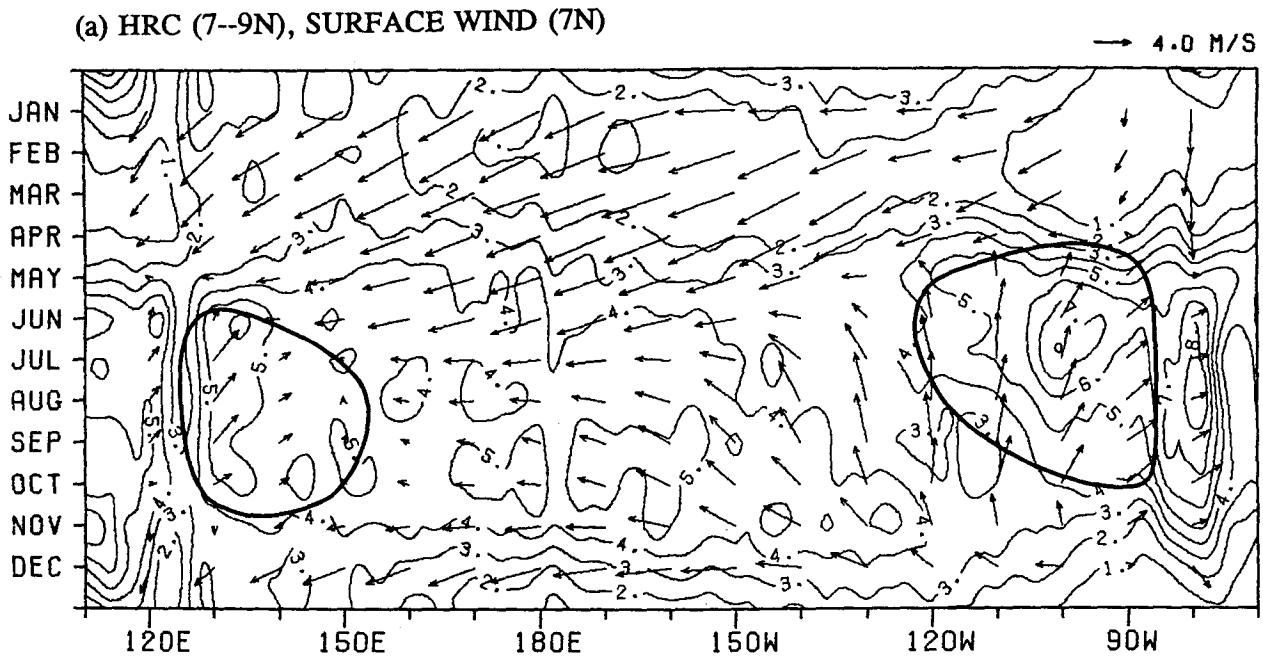

FIG. 8. Climatological monthly HRC (contour) averaged between 7°N and 9°N and the monthly mean surface winds (vector) at 7°N as functions of longitude and month. The heavy solid lines outline summer monsoon rains and associated southwesterlies.

the other hand, easterlies prevail throughout the year with northeast trades in winter and southeast trades in summer. The maximum HRC (4–5 days per month) occurs in October or November with a longer rainy season from May to December and a short dry season from January to March. This part of the ITCZ shows a typical TWCZ regime.

6. Discussion

The most important climate factors that control the annual variation of tropical convection are the annually varying thermal contrast between land and ocean and the annual cycle of SST. The former dominates over continents and adjacent oceans and has been extensively discussed in the monsoon literature (Chang and Krishnamurti 1987; Fein and Stephens 1987). The following discussions will, therefore, focus on and substantiate the importance of SST effects in the formation of the climate regimes of tropical convection.

Most marine arid and semiarid regions are found over relatively cold water: the Pacific and Atlantic cold SST tongues, and the cold water in the Arabian Sea and western equatorial Indian Ocean. In sharp contrast, two massive areas of permanent and semipermanent convective regions are located over the warmest equatorial western Pacific and eastern Indian oceans. This agrees with the observation that deep convection tends to occur where SST is higher than 28°C (e.g., Graham and Barnett 1987; Gutzler and Wood 1990). Similarly, the trade-wind convergence zones of the central Pacific and Atlantic coincide with the underlying warm equatorial countercurrent. Finally, the large-scale inhomogeneity of the underlying SST, that is, the thermal contrast between the cold tongues and the warm pools determines, to a large extent, the location and intensity of the major Pacific convergence zones (the ITCZ and SPCZ). This has been demonstrated by Wang and Li (1993) using a tropical atmospheric model forced by SST.

Although major summer monsoons are basically attributed to the thermal contrast between landmass and oceans, the development of the eastern North Pacific summer monsoon appears to be driven by the strong SST gradient north of the equatorial cold tongue (Murakami et al. 1992). The onset of the monsoon in May was shown to be primarily associated with the reversal of meridional SST (and thus pressure) gradient between the equator and 15°N due to the reestablishment of the Pacific cold tongue (Wang 1992). The interaction between meridional wind and SST gradient may be responsible for the development of the monsoon–cold tongue complex as suggested by Mitchell and Wallace (1992).

The influences of SST on the phase and phase propagation of the wet season are also evident. In the central North Pacific the peak wet season in late fall lags the peak warming of the ocean surface by about one month. In the equatorial eastern Pacific and Atlantic oceans, both the lowest OLR and maximum HRC occur in March–April in accord with the annual peak warming of the ocean surface. The northwestward

propagation of the peak wet season over South and Central America (route 1A on Fig. 3) is nearly in phase with the annual march of peak warming in the adjacent Pacific Ocean (figure not shown). In the northern Indian Ocean and Bay of Bengal, the annual maximum warming of seawater occurs just prior to the monsoon onset.

In summary, the annual variations in land–ocean thermal contrast and SST distribution are fundamental to the annual cycle of the tropical convection. The annual variation of SST, however, is strongly affected by the atmospheric circulation driven by the convection. It follows that the annual variation of the tropical convection should be viewed as a result of the atmosphere–ocean–land interaction in the presence of external insolational forcing.

The information derived from the present analysis will be useful for verification of GCM and climate models in simulating seasonal patterns of tropical convection/rainfall and for better understanding of physical processes responsible for the annual variability of convection. The latter is essential for improvement of the physics of numerical models. In view of the considerable uncertainty in satellite estimates of rainfall and convection, however, the conclusions reached in the present analysis are more qualitative than quantitative. In addition, the climate regimes are identified based upon only the temporal structure of the annual cycles. Future studies of the spatial structure of the cloud systems are needed to verify or improve the present classification.

Acknowledgments. The author is indebted to Drs. T. Murakami and T. A. Schroeder for their comments on an earlier version of the manuscript and to Mr. Z. Tang for his assistance in data processing. The author deeply appreciates anonymous reviewers' relevant comments, which led to an improved presentation of the paper. This research was supported by NOAA EPOCS program and the Office of Naval Research under Grant N00014-90-J-1383.

REFERENCES

Arkin, P. A., Ardanuy, P. E., 1989: Estimating climatic-scale precipitation from space: A review. *J. Climate,* **2,** 1229–1238.

Chang, C.-P., and T. N. Krishnamurti, Eds, 1987: *Monsoon Meteorology.* Oxford University Press, 544 pp.

Dorman, C. E., and R. H. Bourke, 1979: Precipitation over the Pacific Ocean, 30°S to 60°N. *Mon. Wea. Rev.,* **107,** 896–910.

——, and ——, 1981: Precipitation over the Atlantic Ocean, 30°S to 70°N. *Mon. Wea. Rev.,* **109,** 554–563.

Fein, J. S., and P. L. Stephens, Eds, 1987: *Monsoons.* John Wiley and Sons, 632 pp.

Garcia, O., 1985: *Atlas of Highly Reflective Clouds for the Global Tropics: 1971–1983.* U.S. Dept. of Commerce, NOAA, Environmental Research Lab., 365 pp.

Graham, N. E., and T. P. Barnett, 1987: Sea surface temperature, surface wind divergence, and convection over tropical oceans. *Sciences,* **238,** 657–659.

Gruber, A., and A. F. Krueger, 1984: The status of NOAA outgoing longwave radiation data set. *Bull. Amer. Meteor. Soc.,* **65,** 958–962.

Hastenrath, S. L., 1968: Fourier analysis of central American rainfall. *Arch. Meteor. Geophys. Bioklimatol.,* **B16,** 81–94.

Heddinghaus, T. R., and A. F. Krueger, 1981: Annual and interannual variations in outgoing longwave radiation over the tropics. *Mon. Wea. Rev.,* **109,** 1208–1218.

Horel, J. D., 1982: On the annual cycle of the tropical Pacific atmosphere and ocean. *Mon. Wea. Rev.,* **110,** 1863–1878.

——, A. N. Hahmann, and J. E. Geisler, 1989: An investigation of the annual cycle of convective activity over the tropical Americas. *J. Climate,* **2,** 1388–1403.

Horn, L. H., and R. A. Bryson, 1960: Harmonic analysis of the annual march of precipitation over the United States. *Ann. Assoc. Amer. Geogr.,* **50,** 157–171.

Hsu, C.-P. F., and J. M. Wallace, 1976: The global distribution of the annual and semiannual cycles in precipitation. *Mon. Wea. Rev.,* **104,** 1093–1101.

Kendrew, W. G., 1961: *The Climates of the Continents,* 5th ed., Clarendon Press.

Kilonsky, B. J., and C. S. Ramage, 1976: A technique for estimating tropical open-ocean rainfall from satellite observations. *J. Appl. Meteor.,* **15,** 972–976.

Meehl, G. A., 1987: The annual cycle and interannual variability in the tropical Pacific and Indian ocean regions. *Mon. Wea. Rev.,* **115,** 27–50.

Mitchell, T. P., and J. M. Wallace, 1992: Annual cycle in equatorial convection and sea-surface temperature. *J. Climate,* **5,** 1140–1156.

Mokhov, I. I., 1985: Method of amplitude-phase characteristics for analyzing climate dynamics. *Meteor. Gidrol.,* **5,** 80–89.

Morrissey, M. L., 1986: A statistical analysis of the relationships among rainfall, outgoing longwave radiation and the moisture budget during January–March 1979. *Mon. Wea. Rev.,* **114,** 931–994.

Motell, C. E., and B. C. Weare, 1987: Estimating tropical Pacific rainfall using digital satellite data. *J. Climate Appl. Meteor.,* **26,** 1436–1446.

Murakami, T., and B. Wang, 1993: Annual variation of the equatorial east–west circulation over the Indian and Pacific Oceans. *J. Climate,* **6,** 932–952.

——, B. Wang, and S. W. Lyons, 1992: Summer monsoons over the Bay of Bengal and the eastern North Pacific. *J. Meteor. Soc. Japan,* **70,** 191–210.

Ramage, C. S., 1971: *Monsoon Meteorology.* Academic Press, 296 pp.

Reed, R. K., and W. P. Elliott, 1973: Precipitation at ocean weather stations in the North Pacific. *J. Geophys. Res.,* **78,** 7087–7091.

Sadler, J. C., 1975: The upper tropospheric circulation over the global tropics. Report UHMET 75-05, Dept. of Meteorology, University of Hawaii, 35 pp.

——, M. A. Lander, A. M. Hori, and L. K. Oda, 1987: Tropical marine climatic atlas. Vol. 2, Pacific Ocean. Report UHMET 87-02, Department of Meteorology, University of Hawaii, Honolulu, HI 96822, 27 pp.

Scott, C. M., and M. D. Shulman, 1979: An areal and temporal analysis of precipitation in the northeastern United States. *J. Appl. Meteor.,* **18,** 627–633.

Taylor, R. C., 1973: An atlas of Pacific island rainfall. Hawaii Inst. Geophys. Data Rep., 25, HIG-73-9, 175 pp. [NTIS No. AD 767073]

Tucker, G. B., 1961: Precipitation over the North Atlantic Ocean. *Quart. J. Roy. Meteor. Soc.,* **87,** 147–158.

Wang, B., 1992: On the annual cycle of the equatorial Pacific cold tongue. *J. Climate,* submitted.

——, and T. Li, 1993: A simple tropical atmospheric model of relevance to short-term climate variation. *J. Atmos. Sci.,* **50,** 260–284.

Wolter, K., and S. Hastenrath, 1989: Annual cycle and long-term trends of circulation and climate variability over the tropical oceans. *J. Climate,* **2,** 1329–1351.

Yoo, J.-M., and Carton, J. A., 1988: Outgoing longwave radiation derived rainfall in the tropical Atlantic with emphasis on 1983–84. *J. Climate,* **1,** 1047–1054.